ACS Photonics

Article

Cite This: ACS Photonics XXXX, XXX, XXX−XXX

pubs.acs.org/journal/apchd5

Photonic-Crystal-Reflector Nanoresonators for Kerr-Frequency Combs

Su-Peng Yu,*[,†,‡] Hojoong Jung,[†,‡,¶] Travis C. Briles,[†,‡] Kartik Srinivasan,[§] and Scott B. Papp[†,‡]

[†]Time and Frequency Division, NIST, Boulder, Colorado 80305, United States

[‡]Department of Physics, University of Colorado, Boulder, Colorado 80309, United States

[§]Microsystems and Nanotechnology Division, NIST, Gaithersburg, Maryland 20899, United States

ABSTRACT: We demonstrate Kerr-frequency-comb generation with nanofabricated Fabry−Perot resonators, which are formed with photonic-crystal-reflector (PCR) mirrors. The PCR group-velocity dispersion (GVD) is engineered to counteract the strong normal GVD of a rectangular waveguide, fabricated on a thin, 450 nm silicon nitride device layer. The reflectors enable resonators with both high optical quality factor and anomalous GVD, which are required for Kerr-comb generation. We report design, fabrication, and characterization of devices in the 1550 nm wavelength bands. Kerr-comb generation is achieved by exciting the devices with a continuous-wave laser. The versatility of PCRs enables a general design principle and a material-independent device infrastructure for Kerr-nonlinear-resonator processes, opening new possibilities for manipulation of light. Visible and multispectral-band resonators appear to be natural extensions of the PCR approach.

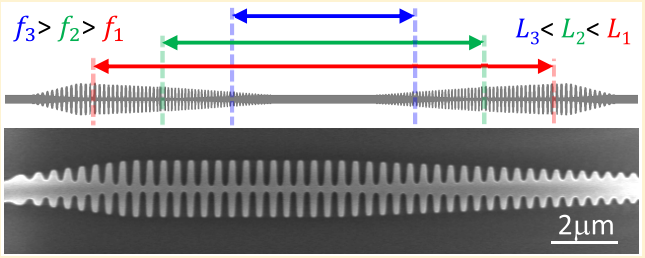

KEYWORDS: *photonic crystal, microresonator, dispersion engineering, nonlinear optics, Kerr effect, frequency comb*

Optical-frequency combs are a revolutionary technology for research ranging from optical spectroscopy[1] and metrology[2] to optical communication.[3] In particular, nanofabricated-frequency-comb systems would allow for widespread application of frequency-comb techniques, enabled by scalable fabrication. Kerr-microresonator frequency combs (microcombs) realized with integrated photonics are also likely to be a potent propelling force for technologies such as optical waveform generation,[4,5] ranging,[6] inertial navigation,[7] and LIDAR.[8] A variety of microcomb systems, with diverse materials and methods, are under active study.

Silicon nitride (Si_3N_4, hereafter SiN) is a thoroughly studied material for micro- and nanophotonic applications due to its low optical loss[9,10] and compatibility with standard semiconductor manufacturing processes. Additionally, the SiN platform is particularly advantageous for Kerr-frequency-comb generation despite its modest index of refraction, because of its high third-order nonlinearity.[11,12] SiN does not suffer from multiphoton absorption in the near-infrared like silicon.[13] SiN has seen rapid development in recent years, for applications including low-power Kerr soliton formation,[14] supercontinuum generation,[15,16] and portable, integrated frequency-comb source.[17]

The challenge for Kerr combs in the ring resonator geometry lies in control of group-velocity dispersion (GVD, or simply dispersion). Typically, photonic waveguides with subwavelength cross-section demonstrate normal GVD associated with index guiding, and this inhibits phase matching of four-wave mixing processes that are necessary for Kerr-comb generation. To maintain anomalous dispersion, a thick SiN device layer is often utilized, leading to challenges in fabrication due to etching thick layers and high material stresses that lead to cracking and low device yield.[18] Additionally, the bulk SiN material demonstrates strong normal dispersion at shorter wavelength ranges,[19] resulting in challenges for Kerr-comb generation with visible light. Methods to alleviate such constraints are under active development, including exotic waveguide geometries[20,21] and novel materials.[22]

In this article, we leverage sophisticated nanofabrication capabilities applicable to SiN photonic devices to create Fabry−Perot-type microresonators with photonic-crystal reflectors (PCRs). Kerr-comb generation can be achieved in Fabry−Perot resonators, provided that a suitable dispersion profile is engineered to enable phase matching.[23] Photonic crystals are periodic dielectric structures demonstrating unprecedented capabilities to engineer optical properties including group velocity[24] and mode profile.[25,26] PCR devices offer targeted optical characteristics derived from nanophotonic patterning, independent of the device layer thickness. The PCR resonator technique offers wide control of dispersion, perhaps enabling use of a wider range of integrated-photonics material platforms for Kerr-comb generation and other nonlinear-optical applications. For application in SiN devices proposed here, the requirement for a thick device layer can be completely alleviated, and the optical properties of such microresonators can be completely controlled by single-layer lithographic patterning. Here we

Received: April 17, 2019
Published: July 8, 2019

DOI: 10.1021/acsphotonics.9b00578
ACS Photonics XXXX, XXX, XXX−XXX

demonstrate high optical quality factor resonators with engineered anomalous dispersion capable of generating Kerr -frequency combs, based on patterned SiN with a 450 nm thickness device layer.

The article is presented as follows: First, we provide an intuitive concept for the PCR resonator Kerr combs, with numerical design methods and a measurement plan; next, we report the fabrication and characterization, followed by a comb-generation experiment; finally, we propose possibilities made available by the PCR technology, including designs for a 532 nm pumped visible-band comb.

DESIGN CONCEPTS

Figure 1(a) presents a conceptual picture of our PCR resonators and their use for Kerr-frequency-comb generation.

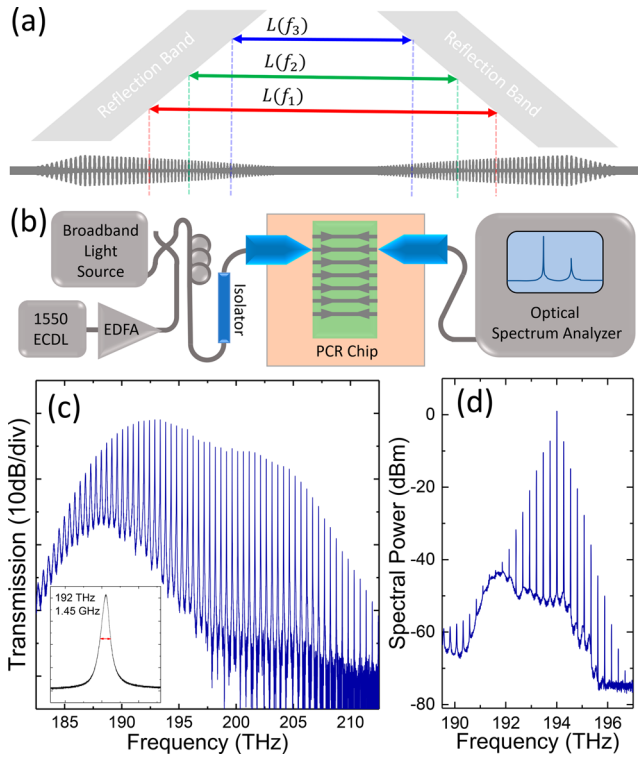

Figure 1. Overview of PCR Kerr-frequency-comb generation. (a) Anomalous GVD engineering in PCRs, with the effective cavity length L decreasing with increasing optical frequency, $f_3 > f_2 > f_1$. (b) Optical testing system, shown with both broad-band and single-frequency light sources. (c) Broad-band transmission spectrum of a device with chirped PCRs demonstrating a ≃20 THz bandwidth and (c inset) laser sweep measurement of a resonance of a nonchirp PCR device with Q = 132 000. (d) Frequency-comb generation by pumping a device with amplified laser light of 1.6 W in the waveguide (Q = 185 000, threshold = 0.75 W).

The resonators are composed of two PCRs, and light is guided between them by a waveguide. Resonator dispersion manifests as a frequency dependence of the free-spectral range (FSR) between adjacent resonances. The free-spectral range has the form FSR = $c/2n_gL$ in a Fabry−Perot resonator, where n_g is the group index. In a Fabry−Perot-type resonator formed with subwavelength cross-section photonic waveguides, strong normal geometric dispersion arises from gradual concentration of the optical field into the high-index waveguide region as the wavelength is reduced, therefore increasing n_g of the guided optical mode. In such a normal-dispersion condition, FSR decreases with increasing optical frequency. To counteract decreasing FSR, the frequency-dependent effective cavity length L can also be utilized as a engineerable parameter. We design PCRs to effectively reduce the cavity length L with increasing optical frequency. Specifically, a PCR can be designed to reflect light at varying depth, with the highest optical frequencies reflecting at the shallowest depth. This is achieved by varying the local bandgap structures on the PCR (gray-shaded areas in Figure 1(a)). The total GVD of a PCR resonator is a combination of the PCR contribution and the waveguide contribution, which scales directly with the waveguide length. Therefore, we may adjust the total dispersion simply by changing the length of the resonator.

OPTICAL CHARACTERIZATION

Figure 1(b) presents the experimental setup we use to characterize both passive device properties, such as broadband on-resosance transmission (c), and to observe Kerr-comb formation (d). In particular, broadband transmission measurements offer a rapid testing procedure to explore the parameter space for PCR designs. We use an unseeded semiconductor optical amplifier as a broadband light source, and a polarization controller and lensed fibers are used to launch light onto the silicon chip. The transmitted light is directly fed into an optical-spectrum analyzer (OSA). The PCR resonators transmit only on resonance, producing a low-background signal on the OSA even for high-Q devices with line width smaller than the resolution bandwidth of the OSA. Fitting the peaks of the broadband spectra allows for rapid extraction of device dispersion information. We are able to efficiently screen through devices to find ones with the desired reflection band wavelength and dispersion profile.

Selected PCR resonators are tested in detail with a tunable laser for accurate determination of quality factor, Q, and resonator external-coupling condition, shown in the inset of Figure 1(c). We characterize the relative strength of the PCR loss channels by measuring the resonance line width and contrast for a variety of devices. We distinguish PCR losses (absorption and scattering) from waveguide propagation loss by measuring resonators with different intraresonator waveguide length and identical PCRs. These measurements indicate a waveguide propagation loss of 1.2 dB/cm, which corresponds to a Q of 243 000. We found the propagation loss to be dependent on the PECVD and annealing conditions for the oxide cladding and could be further optimized in future work. We then analyze the resonance contrast for short devices with varying PCR reflectivity to isolate transmission loss from total device loss, obtaining a loss-limited Q of 107 000 for such devices. Using $Q_{\text{Loss}}^{-1} = Q_{\text{Scattering}}^{-1} + Q_{\text{Absorption}}^{-1}$, we extract an estimation for the scattering-limited Q of 191 000, corresponding to a finesse of 3700 for the 3.8 THz FSR short devices. The scattering-limited finesse is in reasonable agreement with the simulated finesse of 4000 for the nonchirped PCR. We experiment with devices with proper dispersion and high Q factors to create an optical-frequency comb from the PCR resonators. The tunable laser is amplified with an erbium-doped fiber amplifier (EDFA) to provide sufficient power to bring the PCR cavities above the comb-generation threshold. An example PCR Kerr comb, analyzed by the OSA, is shown in Figure 1(d).

DOI: 10.1021/acsphotonics.9b00578
ACS Photonics XXXX, XXX, XXX−XXX

PCR DESIGN THROUGH FINITE-ELEMENT SIMULATIONS

Here we present the design procedure for PCR resonators. There are two primary requirements to be satisfied by the PCRs. First, the PCR must show sufficiently high reflectivity at the design wavelength, as characterized by the finesse $F = \frac{\mathrm{FSR}}{\mathrm{FWHM}}$, where in the case of high PCR reflectivity $R \simeq 1$, $F \simeq \frac{\pi}{1-R}$. Due to the relatively low index contrast between SiN and SiO_2, the maximum achievable reflective bandwidth of a nonchirped, index-guided PCR cannot exceed that of a one-dimensional (1D) quarter-wave stack of the same index contrast. In the case of SiN and SiO_2, the bandwidth is limited to 20% of the center frequency (38 THz) without chirping. The limited guided-mode index and bandgap size also impose a limit on the minimum number of unit cells required to achieve a desired reflectivity, creating a minimum PCR length and potentially limiting the range of group dispersion. In practice, we numerically explore for the optimum design of PCR bandwidth, reflectivity, and dispersion.

Second, the PCR must generate anomalous group-delay dispersion (GDD) in the target wavelength ranges. For ease of comparison, the GDD will be converted to an effective GVD over the in-resonator waveguide by GVD = GDD/L. The PCRs are composed of subwavelength unit cells, whose geometry determines the local reflection band of the crystal, shown in Figure 2(a). A PCR is then built from a stack of continuously varying cells. Finite-element method (FEM) tools are employed to explore the parameter space of unit-cell geometry and the reflection and transmission characteristics of a stack of multiple cells.

Figure 2 presents our design process for PCRs to satisfy the requirements for Kerr-comb generation. A typical unit cell dispersion curve is plotted for the 1D Brillouin zone in Figure 2(a), with its geometry and electric field patterns shown in panel (i–iii). Strong reflection is achieved by creating a photonic bandgap, a frequency range where no guided propagation mode exists. The bandwidth and center of the bandgap can be rapidly simulated with a FEM eigenfrequency solver in full 3D, since the simulation volume contains only one unit cell. We rapidly map the bandgap placement as a function of unit-cell geometries using this method. The unit-cell parameters are then used as components to design reflectors made from a stack of varying cells. A typical reflector begins as an unpatterned waveguide, and the photonic crystal is introduced by adiabatic onset of modulation to the local width of the waveguide. For simplicity, we use a linear tapering scheme for the adiabatic onset, where the parameters such as the waveguide width, modulation amplitude, and lattice constant are varied linearly with the tapering parameter η:

$$\vec{v}(\eta) = \vec{v}_0 + \eta(\vec{v}_1 - \vec{v}_0)$$

where $\vec{v}$ represents the list of unit-cell geometry parameters. The local bandgap of such a taper is shown in Figure 2(b), where the unit cell continuously transforms from a waveguide with width = 750 nm and lattice constant = 430 nm ($\eta = 0$) to the nominal cell of minimum width = 200 nm, lattice constant = 480 nm, and modulation peak amplitude of 875 nm ($\eta = 1$). The geometry is designed so that high optical frequencies reflect at shallower depth in the taper and also to ensure the absence of localized resonance modes inside the reflector itself. The latter means that no frequencies pass through two

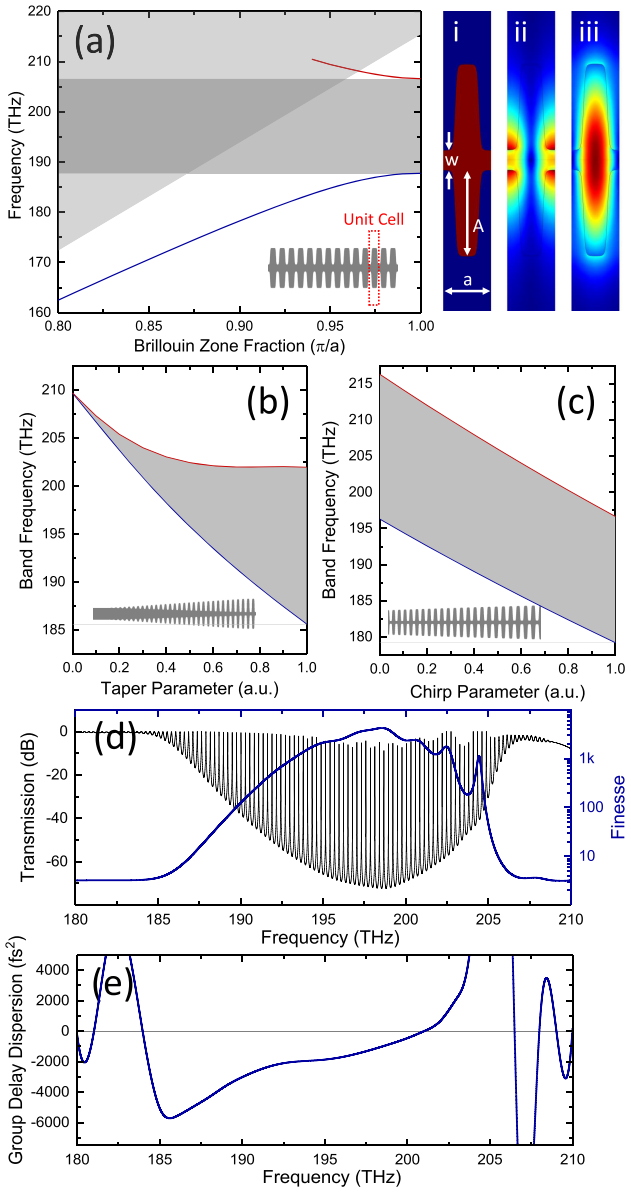

Figure 2. (a) Band structure of the nominal photonic crystal, where a = 450 nm is the lattice constant. At higher frequencies, the upper band (red) couples to free-propagating continuum and is no longer guided. The profiles of (i) the nominal unit cell, minimum width w = 200 nm and modulation A = 875 nm, and the (ii) upper and (iii) lower band electric field are also shown. (b) Local band structures of an adiabatic taper from ordinary waveguide to photonic-crystal reflector. (c) Local band structure of a chirped photonic crystal reflector. (d) Calculated resonator finesse, simulated transmission for a 250 μm resonator, and (e) the group delay dispersion associated with the PCR.

disjointed sections of bandgap on the tapering profile. We also design PCRs with chirped nominal parameters. The scale invariance of Maxwell's equations indicates that a change in reflection wavelength range $\lambda \rightarrow \xi\lambda$ can be achieved by scaling all geometry parameters by $\vec{v} \rightarrow \xi\vec{v}$. In practice, this is carried out for all parameters except the device layer thickness. This chirping scheme enables sweeping of bandgaps over a larger total bandwidth. The local bandgap of this chirped mirror is plotted in Figure 2(c), using the following parameters: the PCR begins with a 750 nm width unpatterned waveguide and a nominal lattice constant of 405 nm. The PCR onset is

DOI: 10.1021/acsphotonics.9b00578
ACS Photonics XXXX, XXX, XXX−XXX

introduced linearly to the nominal dimension of 200 nm minimum width with 875 nm peak-to-peak modulation amplitude at a lattice constant of 455 nm. Then the lattice constant is chirped to 505 nm with the unit cell scaling in the aforementioned manner. The desired anomalous dispersion engineering can be achieved by using either the adiabatic tapering or chirping, or a combination of the two. In the range of parameters we numerically explored, we found the highest simulated finesse to be from nonchirped PCRs. Therefore, the majority of comb-generation devices use the nonchirped design in this study.

With a design in hand, the sweeping trajectory in the parameter space is realized with a finite number of sites, and the resulting stack geometry is simulated in 3D to extract the complex transmission and reflection coefficients of the PCR. With sufficiently slow sweeping of geometry, the scattering loss due to group index and mode profile mismatch can be adiabatically suppressed.[27] A typical simulated finesse curve and an expected transmission are show in Figure 2(d), using the parameters for nonchirped PCR stated previously, with a 30-site tapering, a 10-site nominal PCR unit cell, and 10-site output taper. The reflection coefficient is calculated using a commercial FEM tool (COMSOL Multiphysics) in 3D. The finesse and resonances are then calculated numerically using Matlab approximating the system as a Fabry−Perot resonator with 250 μm length. The trace shows a series of resonances with strong suppression of off-resonance transmission in the target bandwidth from 190 to 200 THz, where anomalous GDD of $\simeq -2000$ fs^2 is generated.

PCR-RESONATOR NANOFABRICATION

We fabricate PCR resonators by the process flow in Figure 3(a). We acquire silicon wafers with thermally grown silicon dioxide for a cladding layer, and the silicon nitride device layer is grown with low-pressure chemical vapor deposition (LPCVD). We choose a device layer thickness of 450 nm to specifically allow for conventional, single-step LPCVD processing and subsequent nanofabrication without the need for stress-relieving patterns,[18,28] annealing steps between multiple LPCVD runs,[19] or other steps necessary to process thick SiN films. The devices are patterned using electron-beam lithography (EBL) and transferred into the device layer using a fluorine-based reactive ion etching (RIE) process. The patterns for the EBL step are adjusted empirically to compensate for dimension changes during pattern transfer, enabling us to fabricate devices in good agreement with the design geometries. We apply a top cladding layer of silicon dioxide, using a plasma-enhanced chemical vapor deposition (PECVD) process, as fully oxide-clad devices enable more efficient input power coupling using lens fibers. Top cladding also makes the devices more robust against contamination. We perform a high-temperature annealing step of 900 °C for 3 h to improve the optical quality of the PECVD oxide after deposition, and we observed up to a factor of 3 reduction of the optical absorption.

To separate chips from the fabrication wafer, we use deep reactive ion etching, which also enables us to fabricate inverse taper bus waveguides, which terminate at the chip facets for high fiber-to-chip coupling efficiency. Overall, we fabricate chips with hundreds of PCR resonator devices, and lensed fiber coupling to the chip devices offers 3.5 dB insertion loss per facet.

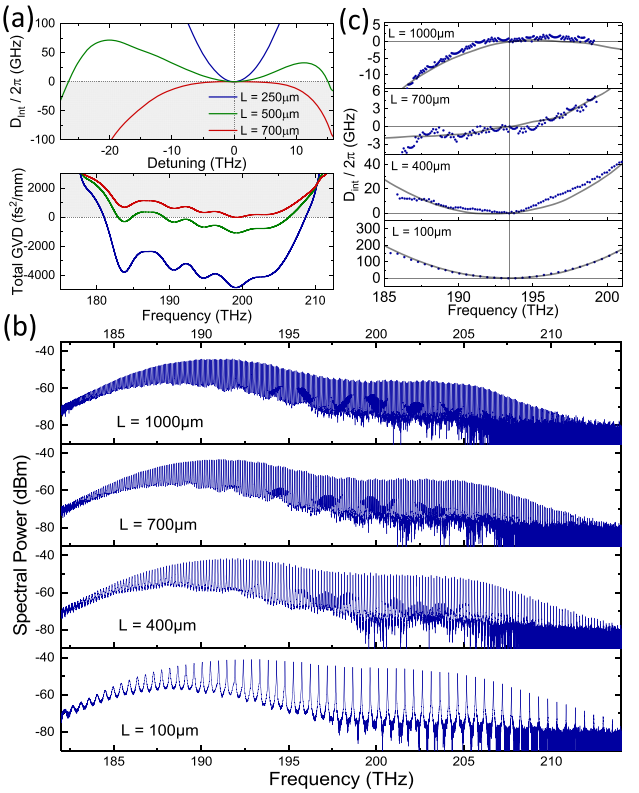

Figure 3. (a) Fabrication process steps include e-beam lithography, pattern transfer by RIE, cladding using PECVD oxide, and chip separation with deep RIE. (b) Stitched-together full view of a resonator and (c) zoom-in image of a photonic crystal reflector using SEM.

PCR-RESONATOR GVD DESIGN AND CHARACTERIZATION

We have carried out a detailed set of simulations to demonstrate GVD engineering in our PCR resonators. With the thin SiN device layer in this study, the total effective GVD is a competition between the normal dispersion of the waveguide and the anomalous effective dispersion of the reflectors. As the length of the resonator is increased, the total effective dispersion continuously varies from strongly anomalous from the reflectors to normal dispersion of the waveguides. Here we engineer the anomalous PCR dispersion using the aforementioned tapering and chirping methods. Following the method mentioned previously, in the following discussion we average the GDD of the PCR over the in-resonator waveguide length. A set of simulated traces demonstrating such dispersion change is plotted in Figure 4(a). Here, the design goal is to form a range of controlled anomalous dispersions around the 1550 nm wavelength band. The resonator length is swept to demonstrate the dispersion balancing, where a near-zero dispersion is predicted at a length of 700 μm.

We can systematically vary the dispersion setting by the tapering condition, with a longer taper resulting in larger anomalous dispersion. Our simulations indicate that a range of dispersion is achievable by this method, although constraints exist from the desire to also achieve high resonator finesse and efficient resonator coupling. Specifically, a taper that is too short in length is no longer adiabatic and causes scattering loss and reduces finesse, while one that is too long results in a

DOI: 10.1021/acsphotonics.9b00578
ACS Photonics XXXX, XXX, XXX−XXX

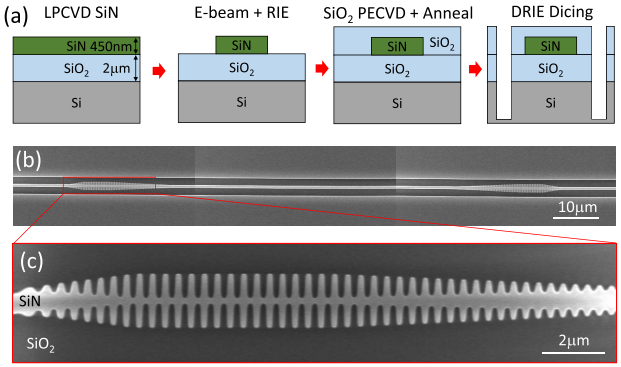

Figure 4. (a) Calculated D_{int} and total dispersion for cavities with a chirped photonic crystal reflector and 500 nm width waveguide of varying length. (b) Measured broadband transmission spectra of chirped reflector and 750 nm width waveguides of varying length, where the FSR are 70, 98, 184, and 484 GHz from panel one (top) through four (bottom), and (c) measured D_{int} from resonance frequencies demonstrating transition from anomalous to normal dispersion. The simulated traces with chirped PCR and 750 nm width waveguide corresponding to the devices in (c) are overlapped for comparison.

reflector with insufficient transmission, hence undercoupling the resonator. For future designs, the restriction associated with insufficient PCR transmission can potentially be alleviated by evanescent coupling the bus waveguide directly to the in-resonator waveguide in a manner similar to the ring resonator case. The strength of normal dispersion of the waveguide section depends on the waveguide width, which can also be varied as a design parameter.

To put PCR-resonator dispersion engineering into practice, we fabricated a series of devices that feature a systematic GVD variation; see Figure 4(b,c). In particular, we design sweeps in device length to demonstrate the counterbalancing of waveguide and reflector dispersion. Transmission measurements using a broadband source, here a supercontinuum source[29] for better measurement bandwidth, allow us to characterize the GVD in detail. The reflecting PCR resonators only transmit light on resonance; therefore the transmission as measured by the OSA comprises a set of narrow peaks; the resulting spectra are shown in Figure 4(b). We identify the frequency of the resonances by finding the peaks of the transmitted power, then calculate the resonator dispersion profiles D_{int}, shown in Figure 4(c). The dispersion profiles demonstrate the predicted gradual transition from strong anomalous dispersion for the $L = 100$ μm to normal dispersion for the longest $L = 1000$ μm case, with the zero-dispersion occurring near $L = 700$ μm.

PCR-RESONATOR KERR-COMB GENERATION

A demonstration of Kerr-frequency-comb generation with PCR resonators is shown in Figure 5. In these experiments, we use a device length of $L_c = 250$ μm, which is within the range described in the previous section. The loaded quality factor of the device is $\geq 10^5$. The specific dispersion parameters of the device are characterized by $D_2 = -c/n \times \beta_2 \times \mathrm{FSR}^2 \approx 2\pi \times 0.45$ GHz/mode, where β_2 is the second-order GVD, and the integrated dispersion $D_{int} = \frac{D_2}{2}m^2 + O(m^3)$, where m is the mode index; see Figure 5(a). We amplify the continuous-wave (CW) pump laser and couple up to 1.6 W onto the chip containing the first PCR. At the parametric-oscillation threshold (as low as 0.75 W on-chip), we observe the

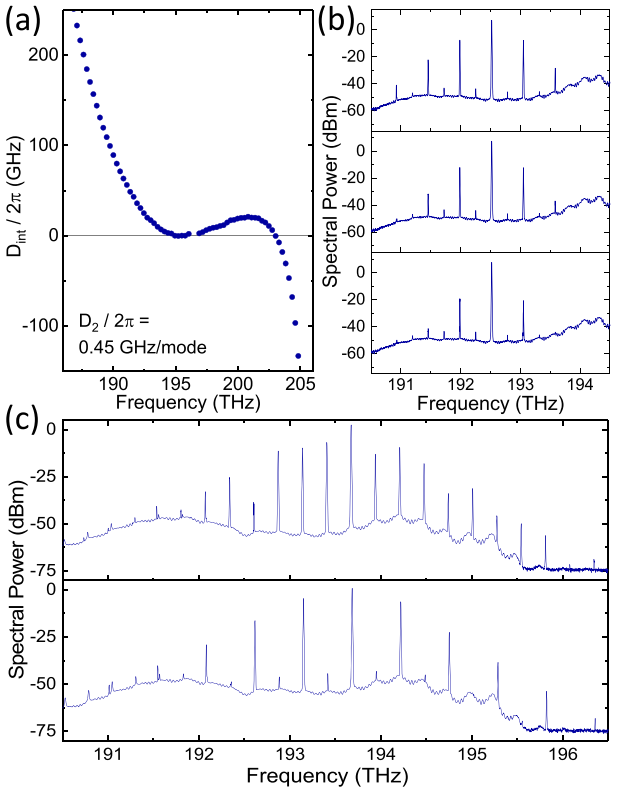

Figure 5. (a) Calculated integrated dispersion D_{int} relative to the pumped mode at 1550 nm. Here the device reflection band is chosen to be off-center from the pump to achieve the desired coupling condition, leading to the asymmetric shape in D_{int}. (b) Onset of primary comb and (c) filling to a full comb with increasing pump detuning. We note that traces in (b) and (c) were measured from two different devices. The PCRs are nonchirped with a 30-cell tapering and 10-cell nominal reflectors. The in-resonator waveguide is 750 nm in width and 250 μm in length, resulting in a 267 GHz FSR. The lattice constant tapering is (b) 430 to 480 nm and (c) 435 to 485 nm, and the pump mode quality factors are (b) 102 000 and (c) 142 000, resulting in threshold powers of (b) 1.62 W and (c) 0.92 W. The filled-in trace in (c) is taken at 1.6 W.

formation of a Kerr comb excited from vacuum noise in the modulation instability regime.

Figure 5(b,c) show the evolution of comb generation, operationally, as we increase the in-resonator power by tuning the CW laser onto resonance. We observe Turing-pattern generation—so-called primary comb—in modes ±2 FSRs away from the pump mode. Harmonics of the primary comb lines become populated with increasing in-resonator power, shown in Figure 5(b). We also observe filling-in of the comb lines to form a full 1-FSR (268 GHz) comb, given sufficient power, shown in Figure 5(c). The elevated background noise level in this figure is the amplified spontaneous emission noise from the amplifier used with the CW laser. The comb generation unambiguously verifies the creation of anomalous dispersion in the PCR resonators. The kinds of Turing patterns that we observe are the fundamental process of any Kerr microresonator. Our experiments show the opportunity to systematically vary the optical-mode spacing of Turing patterns, which offers functionality to generate millimeter-wave electronic signals through photodetection. Moreover, access to Turing patterns offers the possibility for optical-parametric amplification processes of external fields injected to

DOI: 10.1021/acsphotonics.9b00578
ACS Photonics XXXX, XXX, XXX−XXX

the PCR resonator and related optical-wavelength translation processes. In future device fabrication iterations, we plan to target higher Q factors that can both lead to lower threshold and potentially access Kerr-soliton generation.

FUTURE PROSPECTS

We would like to emphasize that a significant advantage of PCR-based resonators is the decoupling of device layer configuration from dispersion engineering. To demonstrate this capability, we utilize the same design principle as the 1550 nm band devices described above to create anomalous dispersion for multiple wavelength bands. An interesting case is shown in Figure 6(a,b), where anomalous dispersion is

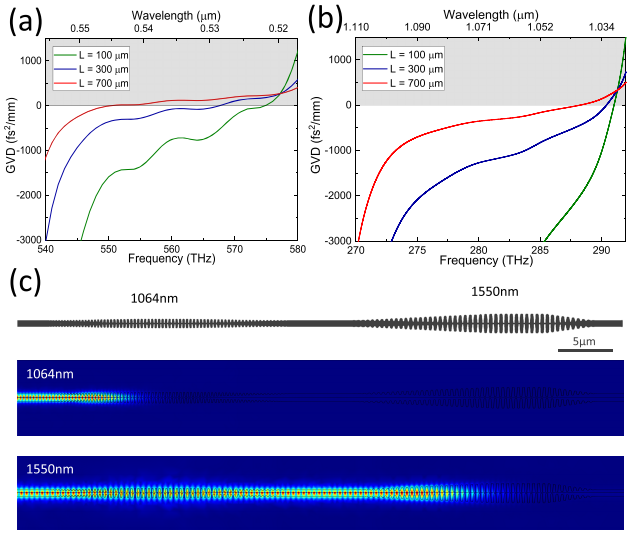

Figure 6. (a) Total dispersion for photonic resonators optimized for anomalous dispersion at 532 nm wavelength and (b) 1064 nm wavelength. (c) Illustration and simulated electric field profiles for 1064 to 1550 nm cascaded photonic crystal reflectors.

created around 532 and 1064 nm wavelength ranges, using a shared SiN device layer thickness of 450 nm. The strong anomalous dispersion of the PCR is sufficient to balance the typically strong normal dispersion of materials in the visible ranges. The capability to engineer dispersion profiles independent of device layer enables integration of multiple wavelength band devices onto the same chip. Taking this concept further, we point out that the PCR is transparent to frequencies below its bandgap, making it possible to build cascaded reflectors like the case shown in Figure 6(c). Silicon nitride has low absorption for both 1550 and 1064 nm wavelengths, enabling dual-wavelength design. The simulated finesses for the 1064 and 1550 nm modes are 4100 and 170, respectively. The optimization for the 1064 nm PCR is more challenging, as it must simultaneously provide desired dispersion properties while minimizing scattering loss for the 1550 nm mode. Multifrequency cascaded resonators as such can potentially provide enhancement for second- or third-harmonics generation or facilitate interlocked combs between different wavelength ranges.[20] The PCR resonators provide flexibility in dispersion control beyond conventional ring and disc resonators and make available dispersion parameter ranges previously difficult to reach.

CONCLUSION

We have presented on-chip Fabry−Perot-type resonators with tailored dispersion based on PCRs, providing a pathway toward integrated photonics frequency comb generation. Conceptually, the PCRs are the microscopic analogy of chirped dielectric stack mirrors, capable of producing anomalous dispersion based on their geometry, independent of the device layer configuration. We designed and fabricated PCR resonators based on a SiN device layer and standard fabrication techniques. Using a broadband light source and an OSA, we were able to directly verify the dispersion profile of such resonators. Anomalous dispersion of varying strength is created in a 450 nm thickness device layer, which is challenging to achieve with conventional ring resonators. We also demonstrated frequency comb generation in these devices. The PCR cavities provide versatile capabilities in dispersion engineering and should enable construction of on-chip frequency comb sources for a wide range of design wavelengths.

AUTHOR INFORMATION

Corresponding Author

*E-mail: supeng.yu@colorado.edu.

ORCID

Su-Peng Yu: 0000-0003-1348-7447

Present Address

¶Present address: Center for Quantum Information, Korea Institute of Science and Technology, Seoul, South Korea.

Notes

The authors declare no competing financial interest.

ACKNOWLEDGMENTS

Funding provided by DARPA DODOS, Air Force Office of Scientific Research (FA9550-16-1-0016), NIST, and UMD/NIST-CNST Cooperative Agreement (70NANB10H193). We acknowledge the Boulder Microfabrication Facility, where the devices were fabricated. We thank Nima Nader and Jeff Chiles for helpful suggestions, and Tara E. Drake and Jizhao Zang for a careful reading of the manuscript. Mention of specific companies or trade names is for scientific communication only and does not constitute an endorsement by NIST.

REFERENCES

(1) Coddington, I.; Newbury, N.; Swann, W. Dual-comb spectroscopy. *Optica* **2016**, *3*, 414−426.

(2) Spencer, D. T.; et al. An optical-frequency synthesizer using integrated photonics. *Nature* **2018**, *557*, 81−85.

(3) Marin-Palomo, P.; Kemal, J. N.; Karpov, M.; Kordts, A.; Pfeifle, J.; Pfeiffer, M. H. P.; Trocha, P.; Wolf, S.; Brasch, V.; Anderson, M. H.; Rosenberger, R.; Vijayan, K.; Freude, W.; Kippenberg, T. J.; Koos, C. Microresonator-based solitons for massively parallel coherent optical communications. *Nature* **2017**, *546*, 274−279.

(4) Jiang, Z.; Huang, C.-B.; Leaird, D. E.; Weiner, A. M. Optical arbitrary waveform processing of more than 100 spectral comb lines. *Nat. Photonics* **2007**, *1*, 463−467.

(5) Cundiff, S. T.; Weiner, A. M. Optical arbitrary waveform generation. *Nat. Photonics* **2010**, *4*, 760−766.

(6) Trocha, P.; Karpov, M.; Ganin, D.; Pfeiffer, M. H. P.; Kordts, A.; Wolf, S.; Krockenberger, J.; Marin-Palomo, P.; Weimann, C.; Randel, S.; Freude, W.; Kippenberg, T. J.; Koos, C. Ultrafast optical ranging using microresonator soliton frequency combs. *Science* **2018**, *359*, 887−891.

DOI: 10.1021/acsphotonics.9b00578
ACS Photonics XXXX, XXX, XXX−XXX

(7) Li, J.; Suh, M.-G.; Vahala, K. Microresonator Brillouin gyroscope. *Optica* **2017**, *4*, 346−348.
(8) Swann, W. C.; Newbury, N. R. Frequency-resolved coherent lidar using a femtosecond fiber laser. *Opt. Lett.* **2006**, *31*, 823−828.
(9) Ji, X.; Barbosa, F. A. S.; Roberts, S. P.; Dutt, A.; Cardenas, J.; Okawachi, Y.; Bryant, A.; Gaeta, A. L.; Lipson, M. Ultra-low-loss on-chip resonators with sub-milliwatt parametric oscillation threshold. *Optica* **2017**, *4*, 619−624.
(10) Pfeiffer, M. H. P.; Liu, J.; Raja, A. S.; Morais, T.; Ghadiani, B.; Kippenberg, T. J. Ultra-smooth silicon nitride waveguides based on the Damascene reflow process: fabrication and loss origins. *Optica* **2018**, *5*, 884−892.
(11) Tan, D. T. H.; Ikeda, K.; Sun, P. C.; Fainman, Y. Group velocity dispersion and self phase modulation in silicon nitride waveguides. *Appl. Phys. Lett.* **2010**, *96*.061101
(12) Tien, M.-C.; Bauters, J. F.; Heck, M. J. R.; Blumenthal, D. J.; Bowers, J. E. Ultra-low loss Si3N4 waveguides with low nonlinearity and high power handling capability. *Opt. Express* **2010**, *18*, 23562−23568.
(13) Bristow, A. D.; Rotenberg, N.; van Driel, H. M. Two-photon absorption and Kerr coefficients of silicon for 8502200nm. *Appl. Phys. Lett.* **2007**, *90*, 191104.
(14) Pfeiffer, M. H. P.; Herkommer, C.; Liu, J.; Guo, H.; Karpov, M.; Lucas, E.; Zervas, M.; Kippenberg, T. J. Octave-spanning dissipative Kerr soliton frequency combs in Si3N4 microresonators. *Optica* **2017**, *4*, 684−691.
(15) Carlson, D. R.; Hickstein, D. D.; Lind, A.; Droste, S.; Westly, D.; Nader, N.; Coddington, I.; Newbury, N. R.; Srinivasan, K.; Diddams, S. A.; Papp, S. B. Self-referenced frequency combs using high-efficiency silicon-nitride waveguides. *Opt. Lett.* **2017**, *42*, 2314−2317.
(16) Guo, H.; Herkommer, C.; Billat, A.; Grassani, D.; Zhang, C.; Pfeiffer, M. H. P.; Weng, W.; Brs, C.-S.; Kippenberg, T. J. Mid-infrared frequency comb via coherent dispersive wave generation in silicon nitride nanophotonic waveguides. *Nat. Photonics* **2018**, *12*, 330−335.
(17) Stern, B.; Ji, X.; Okawachi, Y.; Gaeta, A. L.; Lipson, M. Battery-operated integrated frequency comb generator. *Nature* **2018**, *562*, 401−405.
(18) Pfeiffer, M. H. P.; Kordts, A.; Brasch, V.; Zervas, M.; Geiselmann, M.; Jost, J. D.; Kippenberg, T. J. Photonic Damascene process for integrated high-Q microresonator based nonlinear photonics. *Optica* **2016**, *3*, 20−25.
(19) Luke, K.; Okawachi, Y.; Lamont, M. R. E.; Gaeta, A. L.; Lipson, M. Broadband mid-infrared frequency comb generation in a Si3N4 microresonator. *Opt. Lett.* **2015**, *40*, 4823.
(20) Moille, G.; Li, Q.; Kim, S.; Westly, D.; Srinivasan, K. Phased-locked two-color single soliton microcombs in dispersion-engineered Si_3N_4 resonators. *Opt. Lett.* **2018**, *43*, 2772−2775.
(21) Kim, S.; Han, K.; Wang, C.; Jaramillo-Villegas, J. A.; Xue, X.; Bao, C.; Xuan, Y.; Leaird, D. E.; Weiner, A. M.; Qi, M. Dispersion engineering and frequency comb generation in thin silicon nitride concentric microresonators. *Nat. Commun.* **2017**, *8*, DOI: 10.1038/s41467-017-00491-x.
(22) Rabiei, P.; Rao, A.; Chiles, J.; Ma, J.; Fathpour, S. Low-loss and high index-contrast tantalum pentoxide microring resonators and grating couplers on silicon substrates. *Opt. Lett.* **2014**, *39*, 5379−5382.
(23) Cole, D. C.; Gatti, A.; Papp, S. B.; Prati, F.; Lugiato, L. Theory of Kerr frequency combs in Fabry-Perot resonators. *Phys. Rev. A: At., Mol., Opt. Phys.* **2018**, *98*, No. 013831.
(24) Chung, C.-J.; Xu, X.; Wang, G.; Pan, Z.; Chen, R. T. On-chip optical true time delay lines featuring one-dimensional fish-bone photonic crystal waveguide. *Appl. Phys. Lett.* **2018**, *112*, 071104.
(25) Yu, S.-P.; Hood, J. D.; Muniz, J. A.; Martin, M. J.; Norte, R.; Hung, C.-L.; Meenehan, S. M.; Cohen, J. D.; Painter, O.; Kimble, H. J. Nanowire photonic crystal waveguides for single-atom trapping and strong light-matter interactions. *Appl. Phys. Lett.* **2014**, *104*, 111103.
(26) le Feber, B.; Rotenberg, N.; Kuipers, L. Nanophotonic control of circular dipole emission. *Nat. Commun.* **2015**, *6*, DOI: 10.1038/ncomms7695.
(27) Oskooi, A.; Mutapcic, A.; Noda, S.; Joannopoulos, J. D.; Boyd, S. P.; Johnson, S. G. Robust optimization of adiabatic tapers for coupling to slow-light photonic-crystal waveguides. *Opt. Express* **2012**, *20*, 21558−21575.
(28) Luke, K.; Dutt, A.; Poitras, C. B.; Lipson, M. Overcoming Si_3N_4 film stress limitations for high quality factor ring resonators. *Opt. Express* **2013**, *21*, 22829−22833.
(29) Lamb, E. S.; Carlson, D. R.; Hickstein, D. D.; Stone, J. R.; Diddams, S. A.; Papp, S. B. Optical-Frequency Measurements with a Kerr Microcomb and Photonic-Chip Supercontinuum. *Phys. Rev. Appl.* **2018**, *9*, No. 024030.

DOI: 10.1021/acsphotonics.9b00578
ACS Photonics XXXX, XXX, XXX−XXX